Different Approaches for Efficiency Optimization of DFIG Wind Power Generation Systems

Ahmed G. Abo-Khalil, Ali M. Eltamaly, and Khairy Sayed

Abstract The overall efficiency of the DFIG is superior when it is working close to the rated operating point and rated flux level. However, in light loads, optimal efficiency requires operation at a reduced flux level. In this chapter, several algorithms for increasing the steady-state efficiency that integrated with the wind power generation system are proposed. The proposed algorithms are based on the flux-Elevel reduction by calculating the optimum d-axis current and also by estimating the optimum reference rotor d-axis current by using Particle Swarm Optimization-Support Vector Regression (PSO-SVR) algorithm. The PSO is implemented to automatically perform the parameter selection in SVR modeling while the SVR is used to predict the optimum rotor d-axis current corresponding to the minimum total power loss. The input of the SVR is selected to be wind speeds, d-axis current, and generator power loss. The output of the SVR is the reference d-axis current. An experimental setup has been implemented in the laboratory to validate the theoretical development.

A. G. Abo-Khalil (✉)
Department of Electrical Engineering, College of Engineering, Majmaah University, Almajmaah 11952, Saudi Arabia
e-mail: a.abokhalil@mu.edu.sa

Department of Electrical Engineering, College of Engineering, Assuit University, Assuit 71515, Egypt

A. M. Eltamaly
Sustainable Energy Technologies Center, King Saud University, Riyadh 11421, Saudi Arabia
e-mail: eltamaly@ksu.edu.sa

Electrical Engineering Department, Mansoura University, Mansoura 35516, Egypt

K.A. CARE Energy Research and Innovation Center at Riyadh, Riyadh 11451, Saudi Arabia

K. Sayed
Electrical Engineering Department, Faculty of Engineering, Sohag University, Soha 82524, Egypt
e-mail: khairy_sayed@eng.sohag.edu.eg

A. M. Eltamaly et al. (eds.), *Control and Operation of Grid-Connected Wind Energy Systems*, Green Energy and Technology,
https://doi.org/10.1007/978-3-030-64336-2_2

1 Introduction

The increased energy consumption resulting from high industrial and population growth coupled with the issue of fossil fuel depletion has urgently demanded measures for future energy sources. Many compounds, including carbon dioxide, generated from power generation from fossil fuels pose a threat to the environment, and nuclear developments are not as reliable as they were in the aftermath of earthquakes in Japan. Paying attention to these problems, many research institutes are working to prepare measures at the global level, and the best solution is to introduce a development facility using renewable energy resources such as solar power, wind power, and wave power to replace the dependency on fossil energy sources. Despite comparatively high initial investments, the facilities using alternative energy are boldly under the government's initiative in many countries including developed countries in terms of fossil energy depletion and environmental pollution [1–3].

Among all renewables, wind energy is more economic and for this reason, it has been developed at a commercial level. However, the fixed- speed turbines are ineffective because it means that it is only possible to obtain the best power at a certain speed [4]. To solve this problem, the best solution is a variable speed wind energy development system that changes the speed of a turbine according to the external wind.

Currently, the variable speed turbines are the most used because they optimize the capture of wind and consequently the generation of energy in a wide range of variation of the wind speed. In case of very high wind speed, it is necessary to waste the excess of this one to avoid damages that compromise the physical integrity of the electromechanical conversion system. All turbines are, therefore, designed with some kind of control over the power to be converted. There are two types of control, they are stall control and pitch control, which control the movement around the longitudinal axis of the turbine blades. Among the existing concerns with the integrity of the electrical power system is frequency control. It is known that the frequency of the system is intrinsically linked to the flow of active power, and it is important to keep power generation in constant control. The system must have a power reserve so that it can provide frequency control.

In cases where the adopted configuration consists of using a doubly fed induction generator (DFIG), there is the advantage of being able to increase the injected power by controlling the electromagnetic torque that is generated. The stator winding of the DFIG is connected directly to the power system, while the rotor is connected to the system through a back-to-back converter. This method can supply the power to the system at a constant voltage and frequency even if the speed of the rotor changes with the wind speed [5, 6].

Recently, the use of DFIG has been well established, due to its capability to operate at a variable speed ranging from sub-synchronous speed to super-synchronous speed [7–9]. In the DFIG wind turbine system, as shown in Fig. 1, a back-to-back converter with about 30% of the total capacity exists between the grid and the rotor winding. The converter operates at the slip frequency of ±30% slip and the converter controls

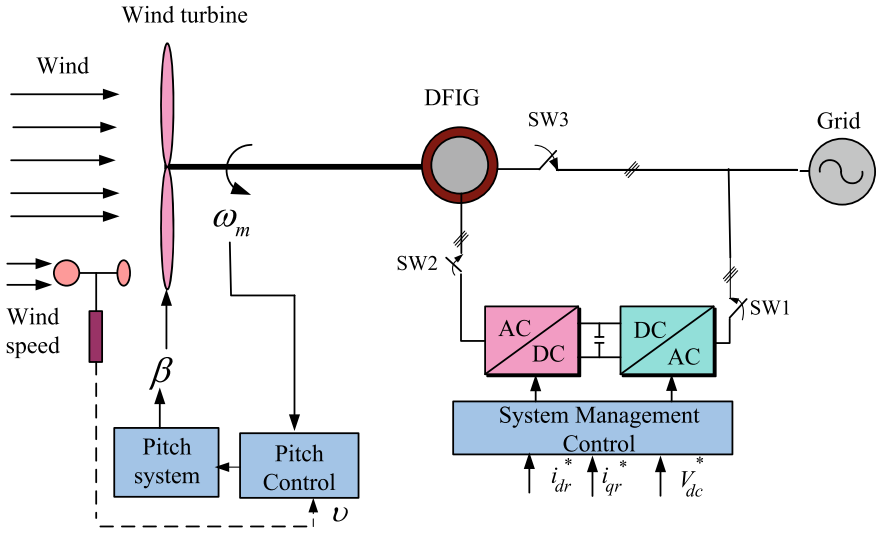

Fig. 1 The basic configuration of the DFIG wind turbine [19]

only the slip power. The converter excites the rotor side to control the wind turbine's output to generate and to control the reactive power and active power of the DFIG. In particular, DFIG's wind turbines are geared up to achieve maximum output [10–12].

Recently, improving the generator efficiency and minimizing the total losses getting more attention. The generator losses can be categorized as electrical copper losses, iron losses, mechanical and stray losses. The first two losses comprise about 80% of the total losses [13]. Generally, the generator flux is set to the rated value to have the best transient response and maximum torque capability. However, this condition increases the generator's total losses at low wind speed. When the generator runs at low speeds, the iron loss increases leading to a decrease in the total unbalance between copper and the iron loss. To control and minimize the total losses at low speeds, the generator flux should be optimized. The wind generator runs most of the time at low speed since the wind speed is lowered the rated value. In this case, the DFIG flux can be reduced by reducing the rotor d-axis current to reduce both copper and iron losses. Several loss minimization control schemes for induction machines using reduced flux levels have been reported in the literature. Many researchers have explored this principle and various methods have been proposed to obtain optimal control of the air-gap flux, especially for machines operating at light loads.

Several studies have presented different methods to improve the DFIG efficiency which can be classified into three categories. The first one is based on the DFIG model [14, 15], which determines the optimum rotor d-axis current by computing losses. The voltage, current, and flux equations are used to calculate the generator power and then obtaining the flux level which minimizes these losses. The advantages of this method are fast and smooth convergence. On the other hand, these methods are depending on the generator electrical parameters completely, so the operator needs

accurate knowledge of the generator parameters to get the operating point correctly. Moreover, the operating conditions such as temperature variation and saturation may cause changes in the generator parameters, which may lead to an error in setting the optimum flux [16, 17]. The second category is based on relating the generator output power and d-axis by a given look-up table [18]. At any wind speed, the look-up table is used to determine the optimum d-axis current by interpolating the optimum efficiency operating point. This method needs a long time to search for the optimum flux level, which is not practical in continuously changing wind speed. The third category is the on-line methods, which depend on measuring the instantaneous torque and lowering the electrical output power settles in the maximum value for predetermined torque [19–22]. The advantage of this method is that there is no need to know the generator parameters since this method is based on searching the optimum flux level, and the insensitivity of this method to the generator parameter variations. However, this method is efficient when the generator runs at a constant speed which is not practical in wind power generation. By applying this method in variable wind power generation systems, it produces continuous flux and torque pulsations around the optimum operating point.

This chapter focuses on presenting the different loss minimization techniques on the DFIG system. The experimental setup is presented to validate the different techniques.

2 Losses in Wind Power Generation Systems

Since the Wind Energy Generation System (WEGS) consists of different mechanical components such as drive train gearbox, generator, etc., numerous losses can be found in the system. The total WEGS losses are divided into two main categories, mechanical and electrical losses. A general power flow diagram for a WEGS is shown in Fig. 2.

The gearbox losses are comprised of the gear mesh which depends on the instantaneous transmitted power and the no-load losses which consist of bearing, oil churning, and windage losses. The approximate percentage of the gear losses at rated load for typical large-scale wind turbines are listed in Table 1 [18].

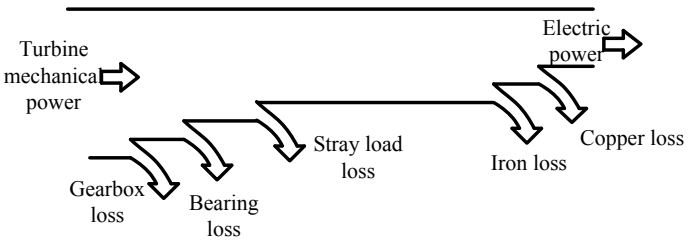

Fig. 2 Power flow in the wind power generation system

Table 1 Losses in the gear at rated load

Friction, windage, and oil churning losses	1.0% include turbine bearing (%)
Gear mesh losses	1.7
Total losses at rated load	2.7

Table 2 Losses in the generators at rated load

	fixed- speed WT	Variable-speed WT	
	IG (%)	Synch. generator (%)	PMSG (%)
Core loss	1.5	1.5	1.5
Cu. Losses, and additional losses	1.5 stator and rotor	1.15 stator	3.5 stator
Friction, windage and cooling losses	0.5	0.5	1.0
Excitation losses	–	0.75	–
Total	3.5	3.9	5.7

The generator losses can be divided into copper, hysteresis, eddy current core, windage, friction, and additional losses. The generator losses are a function of generator current, frequency, flux, and running speed. In large-scale wind turbines, the friction windage and cooling losses are high due to the bearing losses and the large cooling fan. The losses at the rated load of the different generators can be seen in Table 2 [18].

In order to propose a generator loss minimization algorithm in WECS, a relation between the generator losses and wind speed is necessary to be able to perfectly model these losses. It is known that the copper losses decrease in all the generators as the wind speed decreases. The core losses and friction losses are not reduced in the grid-connected induction generator because the flux linkage and the speed remain approximately constant. In the variable-speed systems, the windage and friction losses decrease when the generator speed decreases. The core losses of the directly driven permanent magnet generator do not decrease before the speed is decreased, since the flux linkage is constant. The core losses of the conventional synchronous generator decrease when the wind speed is below 12 m/s, approximate rated wind speed since the flux linkage is reduced by the excitation control. It is known that the generator copper losses decrease much faster than the other types of losses in all the generators. Therefore, the generator iron losses are more significant in the generator total losses than the copper losses in all generators which are used in variable-speed wind turbine systems.

In doubly fed induction generators, the voltage drop across the slip rings can be neglected due to the adjustment of the stator-to-rotor turns so that maximum rotor voltage is 75% of the rated grid voltage to have a safety margin. In Fig. 3, the DFIG losses are shown and it is clear that the generator losses are larger for high wind speeds for the variable speed induction generator (VSIG) system compared to the DFIG system. The reason is that the gearbox ratio is different between the

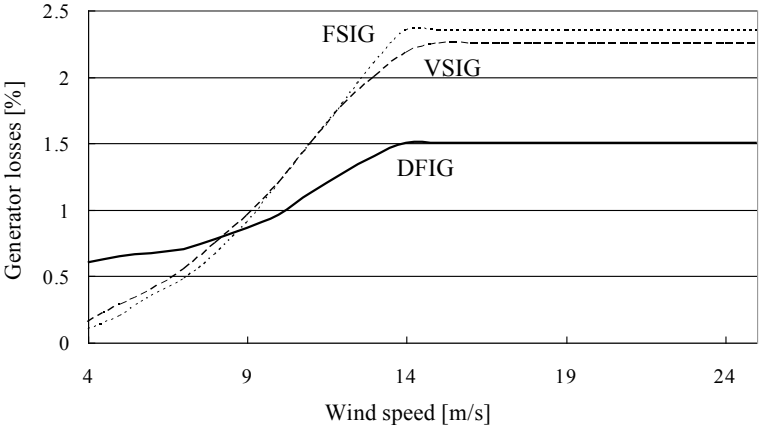

Fig. 3 Generator losses at different wind speed

two systems [23]. It can also be noted that the losses of the DFIG are higher than those of the VSIG for low wind speeds. The reason for this is that the flux level of the VSIG system has been optimized from an efficiency point of view while for the DFIG system the flux level is almost fixed to the stator voltage [24, 25]. This means that for the VSIG system a lower flux level is used for low wind speeds.

3 Losses in Doubly Fed Induction Generator

The generator losses consist of copper loss and iron loss, which are dependent on the current and flux level. At light load conditions, the iron loss can be decreased by reducing the flux level. The power converter losses depend on the current and switching frequency, which is of the lower portion of the total loss and is difficult to control.

3.1 Model-Based Loss Minimization Technique

The d-q equivalent circuits of DFIG considering the stator iron loss are shown in Fig. 4.

The generator copper losses can be expressed as shown in the following equation: [26]

$$P_{cu\_loss} = 1.5(i_{ds}^2 + i_{qs}^2)R_s + 1.5(i_{dr}^2 + i_{qr}^2)R_r \tag{1}$$

where

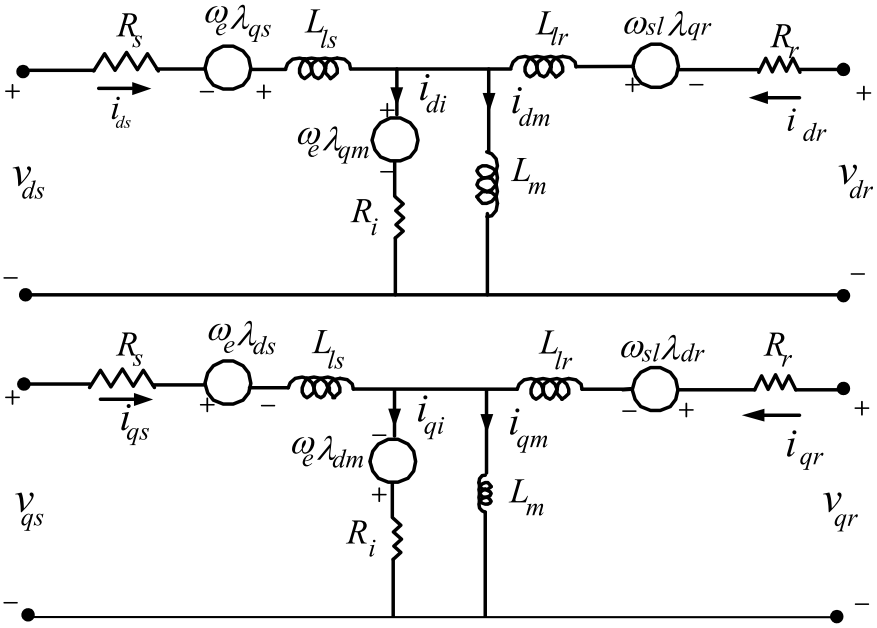

Fig. 4 Equivalent circuits of DFIG

i_{qs} Stator q-axis current [A];
i_{ds} Stator d-axis current [A];
R_s Stator resistance [Ω];
R_r Rotor resistance [Ω];
i_{dr} Rotor d-axis current;
i_{qr} Rotor q-axis current.

Substituting i_{dr} and i_{qr} in (1), copper loss can be expressed as shown in the following equation:

$$\begin{aligned} P_{cu\_loss} = 1.5\,[&(R_s + (L_s/L_m)^2 R_r) i_{ds}^2 - 2\lambda_{ds} L_s R_r i_{ds}/L_m^2 \\ &((T_e/K_t)^2) R_s + (T_e\, L_s/K_t L_m)^2\, R_r) \lambda_{ds}^{-2} \\ &+(\lambda_{ds}/L_m)^2 R_r)\ ] \end{aligned} \tag{2}$$

where
λ_{ds} Stator d-axis flux [Wb];
L_m Magnetizing inductance [H];
T_e Electromagnetic torque.
K_t Torque constant.

To minimize the total copper loss, the derivative of this loss with regard to i_{ds} should be obtained as shown in the following equation:

$$dP_{cu\_loss}/di_{ds} = 3R_s i_{ds} + 3\frac{R_r}{L_m^2}(-L_s\lambda_{ds} + L_s^2 i_{ds}) \tag{3}$$

To represent the DFIG iron loss, resistor R_i is used in the magnetic circuit as shown in Fig. 3 [27]. The stator flux linkages in the d-q reference frame are as

$$\lambda_{ds} = \lambda_{dm} + L_{ls} i_{ds} \tag{4}$$

$$\lambda_{qs} = \lambda_{qm} + L_{ls} i_{qs} \tag{5}$$

In rated torque, the flux is almost constant in d-q reference frame. However, the flux varies slowly according to speed variation when the generator works in the field weakening region [28]. Therefore, the flux variation can be neglected and the current flowing in the core loss branch can be expressed as shown in the following equations:

$$R_i i_{di} = -\omega_e \lambda_{qm} \tag{6}$$

$$R_i i_{qi} = \omega_e \lambda_{dm} \tag{7}$$

where R_i iron loss resistance.

Using (6) and (7), the current flowing in the core loss branch can be expressed as shown in the following equations:

$$i_{di} = -\omega_e(\lambda_{qs} - L_{ls} i_{qs})/R_i \tag{8}$$

$$i_{qi} = \omega_e(\lambda_{ds} - L_{ls} i_{ds})/R_i \tag{9}$$

The generator iron losses can be expressed as shown in the following equation:

$$P_{iron\_loss} = 1.5(i_{di}^2 + i_{qi}^2)R_i \tag{10}$$

Substituting (8) and (9) into (10) the generator iron losses can be expressed as shown in the following equation:

$$P_{iron\_loss} = 5\left[(L_{ls} i_{qs})^2 + \lambda_{ds}^2 - 2\,L_{ls} i_{ds}\lambda_{ds} + (L_{ls} i_{ds})^2\right]\omega_e^2/R_i \tag{11}$$

By substituting i_{qs} into (11)

$$P_{iron\_loss} = 1.5\left[(L_{ls} i_{ds})^2 + \lambda_{ds}^2 - 2\,L_{ls} i_{ds}\lambda_{ds} + (L_{ls} T_e/K_t)^2 \lambda_{ds}^{-2}\right]\omega_e^2/R_i \tag{12}$$

With the same concept, the derivative of iron losses can be taken with regard to the d-axis current as shown in the following equation:

$$dP_{iron}/di_{ds} = 3\frac{\omega_e^2}{R_i}(L_{ls}^2 i_{ds} - L_{ls}\lambda_{ds}) \tag{13}$$

To minimize the total loss, the sum of the derivatives should be equal to zero as shown in the following equation:

$$d(P_{cu\_loss} + P_{iron\_loss})/di_{ds} = 0 \tag{14}$$

The derivative of the total losses can be expressed as shown in the following equation:

$$3\ [(R_s + (L_s/L_m)^2 R_r + \omega_e^2 L_{ls}^2/R_i) i_{ds}\ \ - (\omega_e^2 L_{ls}/R_i\ + L_s R_r/L_m^2)\ \lambda_{ds}\ ]\ \ = 0. \tag{15}$$

After separating i_{ds} from the other variables, the stator d-axis current reference for minimum losses is given by

$$i_{ds}^* = \frac{(L_s R_r R_i + L_m^2 \omega_e^2 L_{ls})\lambda_{ds}}{L_m^2 R_s R_i + L_s^2 R_r R_i + L_m^2 \omega_e^2 L_{ls}^2} \tag{16}$$

The reactive power reference can be adjusted based on this value as shown in the following equation:

$$Q_s = \frac{3}{2} v_{qs} i_{ds}^* = \frac{3}{2} \cdot v_{qs} \cdot (v_{qs}/\omega_e - L_m i_{dr})/L_s \tag{17}$$

3.2 Loss Minimization Using PSO-SVR

In this method, instead of calculating the reference reactive power, a relation between the reference *d*-axis current, wind speed, and the minimum power loss in the DFIG are obtained using PSO-SVR. In this method, a prediction of unknown mapping between the inputs and output is conducted by selecting a series of training data. Wind speed, d-axis rotor current, and the total losses are employed as the input of the SVR, and the generator d-axis current reference samples were used as a target to train the SVR off-line. A fundamental interrelation between wind speed and generator d-axis current reference was predicted from the off-line training process. The predicted function and the instantaneous wind speed were then used on-line to determine the unknown d-axis current reference. When this mapping map is well constructed, the target output, which is the rotor *d*-axis current, can be obtained from the constructed relationship between the inputs, which are the wind speed, d-axis current, and power loss. For each sample, the measured wind speed, rotor d-axis current, and calculated DFIG minimum losses are used to be an input of the SVR function, and the predicted

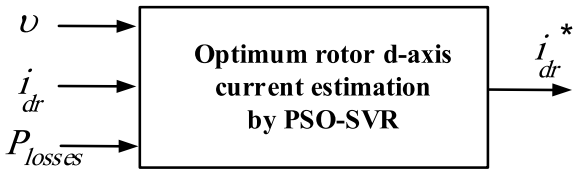

Fig. 5 The structure of the optimum rotor d-axis current estimation

reference d-axis current for minimum losses is the output of the function as shown in Fig. 5.

The details of the proposed loss minimization control are discussed in the next section.

SVR is a regression method that considers the ε-insensitive loss function to predict random real values in the SVM (Support Vector Machine) used to predict the classification problem of training data. SVM is a recent learning method used for binary classification, and it is a technique of classifying data of two groups by obtaining a hyperplane that maximizes margin. Using a learning bias derived from statistical learning theory, a linear virtual space on a high-dimensional feature space that is trained by a learning algorithm will be used. This learning strategy is superior to other methodologies in a wide range of fields.

The purpose of the SVR is to find the hyperplane that minimizes the distance in all data. The regression function f (x) for predicting the optimal hyperplane targeted by the SVR is made as shown in Eq. (18) [28–30] as follows:

$$f(x) = (w^T.\varphi(x)) + b \tag{18}$$

where w^T is the weight vector and b is bias. $\varphi(x)$ is a space in which the vector x of the input space is nonlinearly mapped into a feature space of a high dimension. Including the ε-insensitive loss function and the slack variable ξ allows the optimization problem to be written as shown in Eq. (19) as follows:

$$Min \ \frac{1}{2}\|w\|^2 + \gamma \sum_{i=1}^{n} \Gamma(f(x_i) - y_i) \tag{19}$$

which is subjected to the following condition:

$$\begin{aligned} |y_i - w \cdot \Phi(x_i) - b| \ &\leq \varepsilon + \xi_i \\ i = 1, 2, ...n \quad \xi_i, \xi_i^* &\geq 0 \end{aligned} \tag{20}$$

where γ is a pre-specified value that controls the cost incurred by training errors. The slack variables, ξ_i and ξ_i^*, are introduced to accommodate the error on the input training set. Equation (19), $\frac{1}{2}\|w^2\|$ is a regularized term, ε is the permissible error, γ is a pre-specified value that controls the cost incurred by training errors, and the slack

variables, ξ_i and ξ_i^*, are introduced to accommodate the error on the input training set.

Using the Lagrangian multiplier in Eq. (16), the general form of the SVR-based regression function is derived as follows [31]:

$$f(x) = \sum_{i=1}^{n} (\alpha_i - \alpha_i^*) \times K(x_i, x) + b \tag{21}$$

where α_i and α_i^* are Lagrange multipliers and $K(x_i, x_j) = \Phi(x_i)^T \Phi(x_j)$ is the kernel function.

$$K(x_i, x) = \exp\{-\frac{|x_i - x|^2}{\sigma^2}\} \tag{22}$$

In this study, radial base function (RBF) with [32] K is used as the kernel function, where σ is the RBF width. The parameters to be determined by the user in the SVR are the cost variable γ, the value of the ε-insensitive loss function, and the σ of the RBF. The optimal values of the three parameters were calculated through optimization using PSO.

PSO was first proposed by Kennedy and Eberhart (1995), and it is different from using natural selection evolution such as genetic algorithms. It has a parallelism feature and performs optimization using the concept of Swarm and Particle. Each randomly formed particle in the initial swarm travels the dimensional space by the number of parameters you choose to find the optimal value. After the initial Swarm search, the next Swarm remembers the value of the objective function for the location of each particle and shares the values with other particles to find the optimal solution. These features change from global search to regional search as generations pass and finally, converge to one point to find the optimal solution. In addition, the theory is simpler compared to other algorithms, making it easy to implement and efficient in operation.

In the PSO algorithm, the swarm has n agents specified particles, which is a set of user-selected parameter values. The equation of the PSO algorithm is as follows [33, 34]:

$$\begin{aligned} v_{jk}(t+1) = {} & \omega_{damp} \bullet \omega(t) \bullet v(t) \\ & + c_1 \bullet r_1 \bullet (P_{best,jk}(t) - x_{jk}(t)) \\ & + c_2 \bullet r_2 \bullet (P_{best,k}(t) - x_{jk}(t)) \end{aligned} \tag{23}$$

where v_{jk} is the moving speed of parameter k of the jth particle in the group, ω_{damp} is the damping of the inertia control function,ω is inertia weight, c is acceleration constant, r is a random value, P_{best} is the optimal objective function value of the current swarm (particle), G_{best} is the optimal objective function value in all Swarm, and x_{jk} is the objective function value of the particle currently calculated. Particle

velocity (v_{jk}) is the only operator of the PSO and is a multidimensional real vector representing the velocity of each parameter [35].

Particles in Swarm are used in Eq. (23) and it is generated depending on the speed of each parameter calculated in (23) and has dimensions as many as the number of parameters. Inertial load ω adjusts global search and local search capabilities when particles are formed. Initially, a large value is used to search globally, and as the number of iterations of the algorithm increases, the value of the inertia load decreases to allow a local search. The inertia control function ω_{damp} is a constant for convergence from wide-area search to local search by decreasing the value of inertia as the Swarm generation mentioned above. Acceleration constant c represents the stochastic acceleration of particles toward G_{best} and P_{best}. Smaller values of acceleration constants cause them to wander outside without going to the optimal solution, while higher values of acceleration constants can cause them to jump beyond the optimal solution or cause a sudden change of direction. The value can be between 0 and 1. In this study, the inertia load was set to 0.9, the acceleration constants c_1 and c_2 were set to 1.2, and the inertia control function was set to 0.9.

P_{best} and G_{best} are particles having the optimal values of the objective functions specified by the user among the particles in Swarm, which are the particle best and the global best, and P_{best} is the particle having the most optimal value among all the particles of Swarm. The final G_{best} of the algorithm thus represents the optimal solution of the given parameter. Since there is no G_{best} in the initial particle formation, particles are randomly formed only under the influence of P_{best}, but from the next generation of Swarm, particles are generated based on the previous G_{best} and P_{best} of Swarm.

The PSO algorithm adjusts its position according to the experience of neighboring entities. The entire multidimensional space formed by the parameters selected by the user can be explored. Particles formed in Swarm can be positioned by sharing the value and velocity of the objective function with other particles. Unlike the conventional methodology, the random probability optimization algorithm enables searching in uncertain domains and the calculation of operators is fast, so that an optimal solution can be easily produced. The relationship between global search and local search can be flexibly adjusted using inertial loads. If you are not familiar with model calibration, you can achieve significant accuracy if you only set the appropriate parameters and ranges. However, due to the stochastic approach, it is necessary to run the model more than a certain number of times in order to obtain good calibration results. The user's choice is based on the analysis results [36–38].

In this study, the PSO is implemented in a way to fast tune and optimize the SVR parameters. The framework of a PSO-SVR method is depicted in Fig. 6, which is described as shown in the following points:

(1) Collect training data (x_i, y_i) and determine the parameters ε, C, and σ using PSO.
(2) Determine the kernel function $K(x_i, y_i)$ from the collected data.
(3) Compute the Lagrange multipliers, b, and α_i by minimizing the quadratic function in

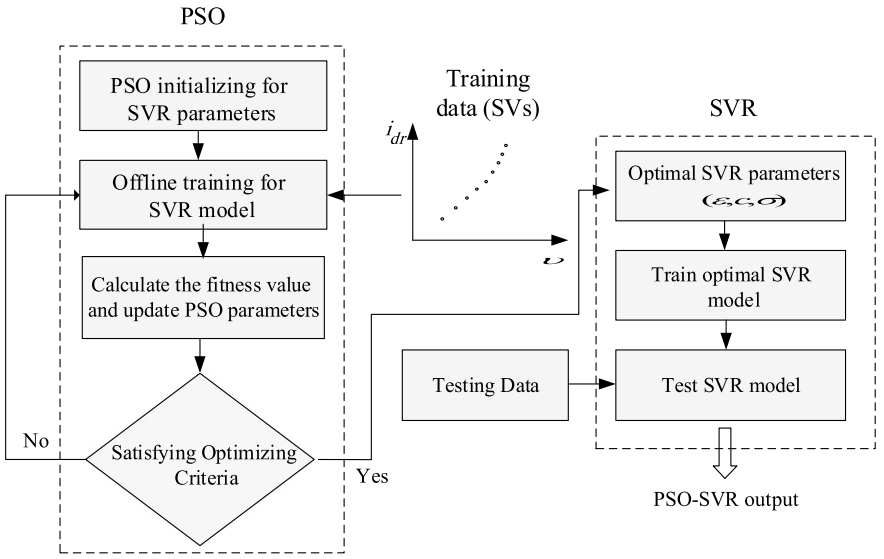

Fig. 6 Flowchart for loss minimization of DFIG using PSO-SVR

$$W(\alpha_i, \alpha_i^*) = \frac{1}{2}\sum_{i,j=1}^{n}(\alpha_i - \alpha_i^*)(\alpha_j - \alpha_j^*)K(x_i, x_j) - \sum_{i=1}^{n} y_i(\alpha_i - \alpha_i^*) + \frac{1}{2C}\sum_{i=1}^{n}(\alpha_i^2 - \alpha_i^{*2}) \tag{24}$$

subject to

$$\sum_{i=1}^{n}(\alpha_i - \alpha_i^*) = 0,\ \alpha_i,\ \alpha_i^* \in [0, C]$$

$$b = mean\left(\sum_{i=1}^{n}\left\{y_i - (\alpha_i - \alpha_i^*)K(x_i, x_j)\right\}\right) \tag{25}$$

All parameters in (25) are already off-line computed.

(4) Calculate the output of the estimator for any input.

Figure 7 shows the PSO-SVR training result for different wind speeds. The red-circled points are the training data which are included as support vector while the black cross points represent the data that are not supported vectors. The solid lines which go through the support vectors represent the learned model.

Figure 8 shows a block diagram of the rotor-side converter which controls the stator active and reactive power [36, 39]. The optimum output power P^* of the DFIG is used as the reference value for the power control loop. In this controller, the outer

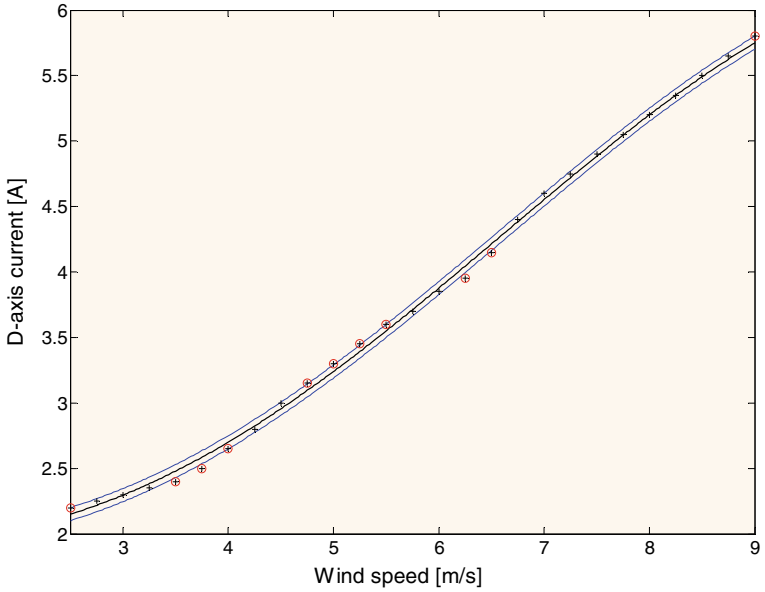

Fig. 7 RBF Kernel regression for d-axis current estimation

stator power control loop produces a reference value, i_{qr}^{*}, for the inner current control loop. The voltage command value generated in the process is implemented through a PWM signal.

The stator reactive power Q_s is controlled to the value to minimize the generator's total losses and to produce the d-axis rotor current reference.

Next, the grid-side converter is shown in Fig. 9. It plays a role in maintaining the DC-Link voltage of the system converter uniformly to transfer the power generated by the DFIG to the system without loss [27, 40–42].

4 Experimental Results

The wind power generator simulator, consisting of DFIG driven by a squirrel-cage induction motor as a wind simulator, was built in hardware and subjected to hardware experiments, as shown in Fig. 10.

To verify the validity of the suggested method, an experimental prototype was built and tested to control a 3-KW induction generator in a wind power generation system. The control algorithm was applied using a TMS320C33 DSP. Thy dynamic and steady-state characteristics of the induction generator with rated and reduced flux levels were tested. The parameters of the wind turbine and DFIG are listed in Tables 3 and 4 in the Appendix.

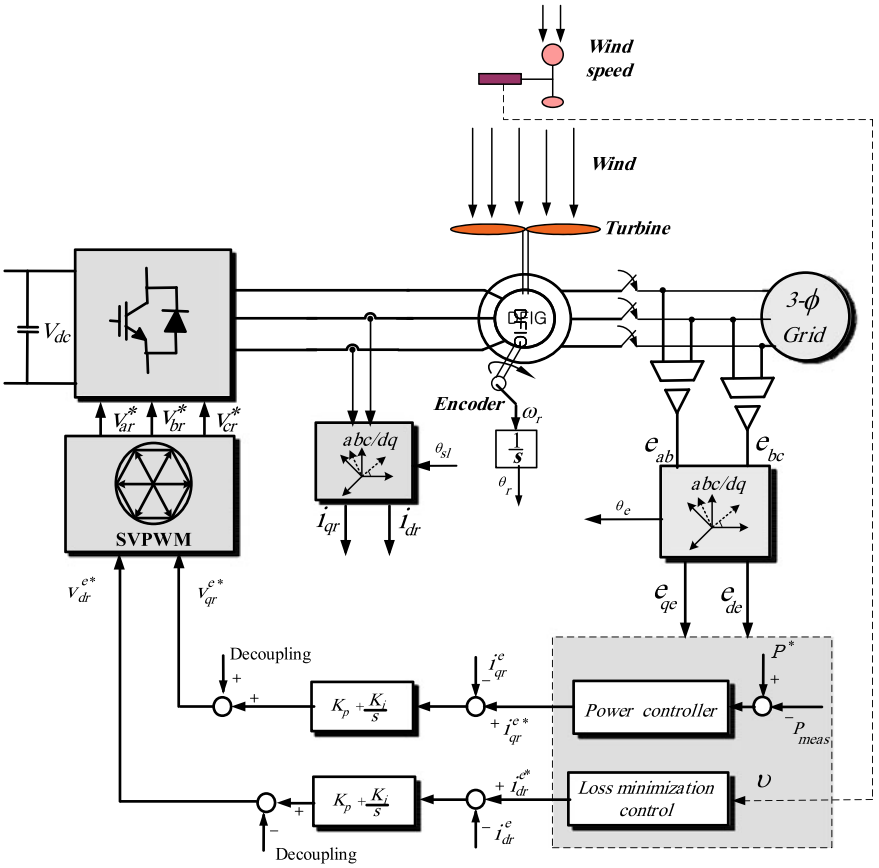

Fig. 8 On-line loss minimization control of rotor-side

Figure 11 gives the generator performance at 6 m/s wind speed. The DFIG is started with the rated flux current, and then the loss minimization algorithm is activated by estimating the optimum d-axis current and adjusting the reference reactive power to the value which reduces the total loss minimization to the minimum value. The calculated reference reactive power is shown in Fig. 11a. The loss minimization reactive power controller produces the optimum rotor d-axis current which decreased from the rated value to the minimum loss value. In this figure, the d-axis current is achieved its a steady-state reduced value of about 3.1A, as shown in Fig. 11b, very fast to achieve the minimum power loss. The stator d-axis current increased as a response of reactive current increasing as shown in Fig. 11c. The average power loss decreased from 128 to 71 W, which means about 43% can be saved. At the same time, the generator output power is increasing due to loss reduction as shown in Fig. 11d.

Figure 12 shows the generator performance at 7 m/s wind speed. The reduced d-axis current, in this case, is a little higher than the 6/s wind speed. The average d-axis

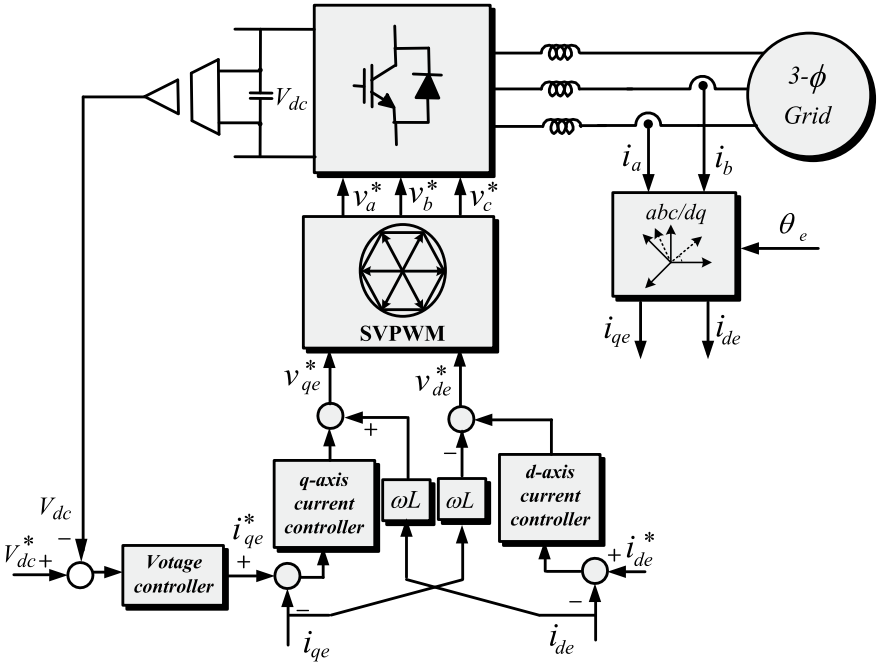

Fig. 9 DFIG grid-side control

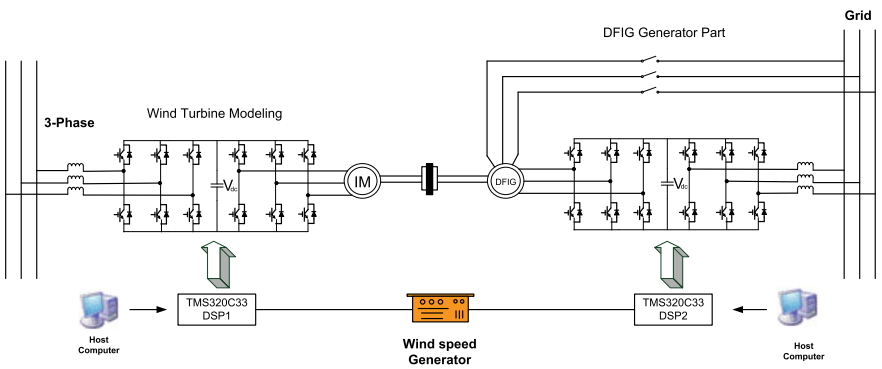

Fig. 10 Schematic of the experimental setup for a DFIG connected to the grid

current reduced steady state is about 3.5A as shown in Fig. 12b. The reduction in the d-axis current causes the increase in the reactive power and stator d-axis current of Fig. 12a and c. The average power loss is decreased also slightly from 150 to 90 W, which means about 40% can be saved in this condition.

As we can notice from Figs. 11 and 12, the power loss reduction is influenced mainly by the wind speed (and generator speed). The loss minimization process is

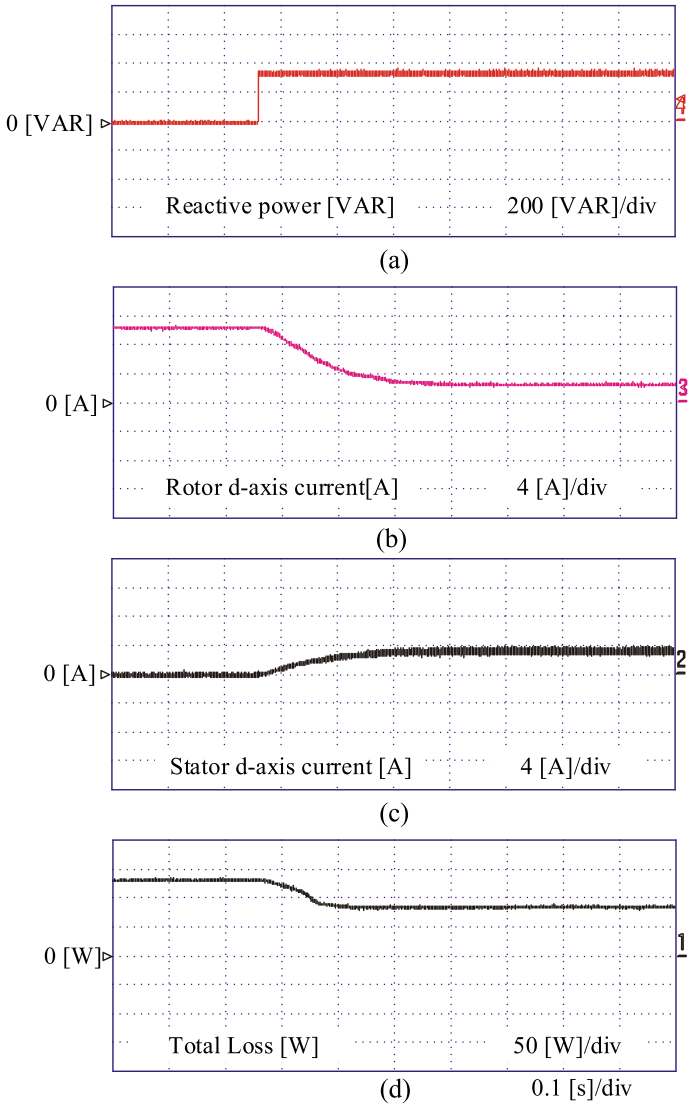

Fig. 11 Loss minimization at 6 m/s

more efficient at low wind speed and the percent of power saving in this rating can be more than 43%. Though this result is well known from the basic principles, it is confirmed that the proposed control algorithm is effective to reduce the induction generator operating loss.

Figure 13 shows the DFIG power loss when using conventional control and using loss minimization control. In very low wind speed, the power saving is higher when the loss minimization controller is activated. As the wind speed increases, the power

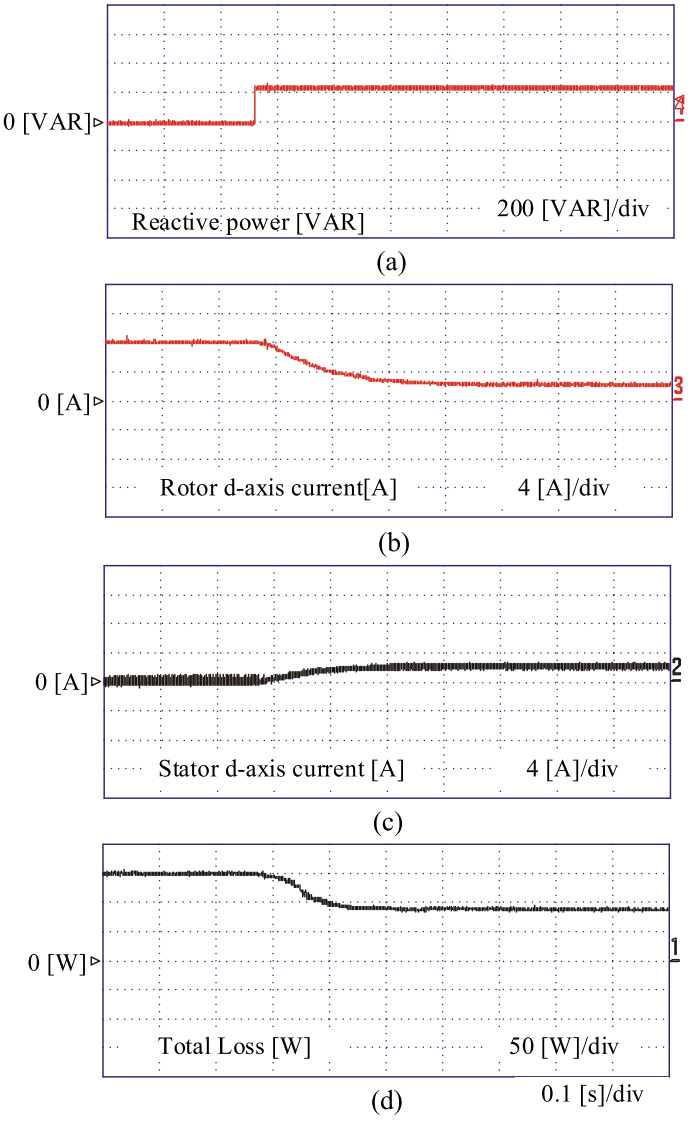

Fig. 12 Loss minimization at 7 m/s

saving decreases since the generator runs near the full load condition where the d-axis current is set to the rated value for high torque.

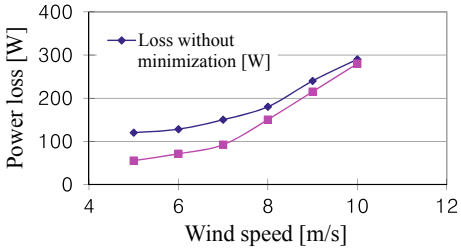

Fig. 13 Generator loss minimization at low speed

Table 3 Parameters 3[kW] double-fed induction machine

Parameters	Value
Stator resistance	0.6 [Ω]
Rotor resistance	0.713 [Ω]
Iron loss resistance	155 [Ω]
Stator leakage inductance	0.003313 [H]
Rotor leakage inductance	0.066756 [H]
Mutual inductance	0.063443[H]

5 Conclusions

Wind power generation systems operate most of the time at a fraction of the rated power due to the low wind speed. This operating condition causes a considerable iron and copper loss, which reduces the total efficiency of the system. The DFIG is usually controlled to extract the maximum power point by controlling the rotor q-axis current while the reactive power is determined to control the generator excitation and the desired grid power factor. The stator and rotor d-axis currents determine the generator excitation level and the level of power loss.

In this chapter, a loss minimization control scheme for wind-driven DFIG was proposed. The stator d-axis current is estimated to minimize the DFIG total losses by controlling both stator's reactive power and rotor d-axis current wither in the constant or variable wind/generator speed. A relationship between the rotor d-axis current, wind speed, and power loss was deduced to calculate the optimum flux level which minimizes the generator total losses. The experiment for 3[kW] has shown that it is possible to reduce the power loss by up to 43% at 6[m/s] wind speed. Finally, this method can be used in large-scale wind power generation systems to minimize the total losses at low wind speed.

Table 4 Parameters of turbine blade model

Parameters	Value
Blade radius	0.95 [m]
Max. power conv. coeff	0.45
Optimal tip-speed ratio	7
Cut-in speed	4 [m/s]

6 Appendices

The specification of the DFIG used for test is three-phase, four poles, 230[V], 60[Hz], 3[kW], of which parameters are listed in Table 3. The parameters of the wind turbine used are shown in Table 4.

References

1. Eltamaly AM (2007) Modeling of wind turbine driving permanent magnet generator with maximum power point tracking system. J King Saud Univ-Eng Sci 19(2):223–236
2. Abo-Khalil AG, Alghamdi A, Tlili I, Eltamaly A (2019) Current controller design for DFIG-based wind turbines using state feedback control. IET Renew Power Gener 13(11):1938–1949
3. Abo-Khalil AG (2012) Synchronization of DFIG output voltage to utility grid in wind power system. Elsevier J Renew Energy 44, 193–198
4. Park HG, Abo-Khalil AG, Lee DC, Son KM (2007) Torque ripple elimination for doubly-fed induction motors under unbalanced source voltage. In: Proceedings of the power electronics and drive systems PEDS,07, pp. 1301–1306
5. Abo-Khalil AG, Kim HG, Lee DC, Lee SH (2006) Grid connection of doubly-fed induction generators in wind energy conversion system. In: Proceeding of 5th international power electronics and motion control conference (IPEMC 2006). Shanghai, China, pp 14–16, 1–5
6. Zhong QH, Ruan Y, Zhao MH, Tan L (2013) Application of variable-step hill climbing searching in maximum power point tracking for DFIG wind power generation system. Power Syst Prot Control 41:67–73
7. Abrahamsen F, Blaabjerg F, Pedersen JK, Thogersen PB (2000) Efficiency optimized control of medium-size induction motor drives. Rome, Italy, IEEE-IAS Annu. Meeting, pp 1489–1496
8. Park HG, Abo-Khalil AG, Lee DC (2008) Wind turbine simulators considering turbine dynamic characteristics. Trans Korean Inst Electr Eng 57(4):617–624
9. Abo-Khalil AG (2015) Control system of DFIG for wind power generation systems. LAP LAMBERT Academic Publishing, ISBN-10: 3659649813, ISBN-13: 978-3659649813
10. Li Y, Xu Z, Zhang J, Wong KP (2018) Variable gain control scheme of DFIG-based wind farm for over-frequency support. Renew Energy 120:379–391
11. Khemiri N, Khedher A, Mimouni MF (2012) Wind energy conversion system using DFIG controlled by backstepping and sliding mode strategies. Int J Renew Energy Res 2:421–430
12. Abo-Khalil AG, Ab-Zied H (2012) Sensorless control for DFIG wind turbines based on support vector regression. In: Industrial Electronics Conference IECON. Canada
13. Abo-Khalil AG, Park H-G, Lee D-C, Ryu S-P, Lee S-H (2007) Loss minimization control for doubly-fed induction generators in variable speed wind turbines. In: ECON 2007-33rd annual conference of the IEEE industrial electronics society, pp 1109–1114
14. Abo-Khalil AG (2011) Model-based optimal efficiency control of induction generators for wind power systems. In: ICIT 2011, pp 191–197

15. Yang S-M, Lin F-C (2001) Loss-minimization control of vector-controlled induction motor drives. IEEE PEDS Conf Proc 1:182–187
16. Abo-Khalil AG, Kim HG, Lee DC, Lee S-H (2004) Maximum output power control of wind generation system considering loss minimization of machines. In: Proceedings of IECON'04, pp 1676–1681
17. Leidhold R, Garcia G, Valla MI (2002) Field-oriented controlled induction generator with loss minimization. IEEE Trans Ind Electron 49:147–156
18. Poitiers F, Bouaouiche T, Machmoum M (2009) Advanced control of a doubly-fed induction generator for wind energy conversion. Electr Power Syst Res 79:1085–1096
19. Lee D-C, Abo-Khalil AG Optimal efficiency control of induction generators in wind energy conversion systems using support vector regression. J Power Electron 8(4):345–353
20. Sousa GC, Bose BK, Cleland JG (1995) Fuzzy logic based on-line efficiency optimization control of an indirect vector-controlled induction motor drive. IEEE Trans Ind Electron 42:192–198
21. Chedid R, Mard F, Basma M (1999) Intelligent control of a class of wind energy conversion systems. IEEE Trans Energy Conv 14(4):1597–1604
22. Abo-Khalil AG, Lee DC (2008) Maximum power point tracking based on sensorless wind speed using support vector regression. In: IEEE Trans Ind Electron 55(3)
23. Grauers A (1996) Efficiency of three wind energy generator systems. IEEE Trans Energy Convers 11(3):650–657
24. Grauers A (1996) Design of direct-driven permanent-magnet generators for wind turbines. Ph.D. dissertation, Chalmers University of Technology, Goteborg, Sweden
25. Peterson A (2005) Analysis, modeling and control of doubly-fed induction generators for wind turbines. Ph.D. dissertation, Chalmers University of Technology, Goteborg, Sweden
26. Abo-Khalil AG, Lee DC, Seok JK (2004) Variable speed wind power generation system based on fuzzy logic control for maximum output power tracking. In Proceeding of power electronics specialists conference, vol 20–25. Aachen, Germany, pp 2039–2043
27. Eltamaly AM, Al-Saud MS, Abo-Khalil AG (2020) Dynamic control of a DFIG wind power generation system to mitigate unbalanced grid voltage. IEEE Access
28. Eltamaly AM, Al-Saud MS, Sayed K, Abo-Khalil AG (2020) Sensorless active and reactive control for DFIG wind turbines using opposition-based learning technique. Sustainability 12(9):3583
29. Eltamaly AM, Alolah AI, Abdel-Rahman MH (2010) Modified DFIG control strategy for wind energy applications. In: Proceeding of power electronics electrical drives automation and motion (SPEEDAM), vol 14–16. Pisa, Italy, pp 653–658
30. Abo-Khalil AG (2015) Control system of DFIG for wind power generation systems. LAP LAMBERT Academic Publishing: Latvia, ISBN-10: 3659649813, ISBN-13: 978-3659649813
31. Abo-Khalil AG, Alyami S, Sayed K, Alhejji A (2019) Dynamic modeling of wind turbines based on estimated wind speed under turbulent conditions. Energies 12(12):1907
32. YU BG, Abo-Khalil AG, Matsui M, Yu G (2009) Support vector regression based maximum power point tracking for PV grid-connected system. In: Photovoltaic specialists conference PVSC 34th. Philadelphia USA
33. Nuller KR, Smola A, Ratrch G, Scholkopf B, Kohlmargen J, Vapnik V (1997) Predicting time series with support vector machine in Pm/CA 1997. Springer LNCS 1327, pp 999–1004
34. Abo-Khalil AG, Lee D-C (2007) DC-Link capacitacne estimation using support vector regression in AC/DC/AC PWM converters. Korean Inst Electr Eng J 56(1):81–87
35. Abo-Khalil AG, Lee D-C (2008) DC-Link capaciance estimation in AC/DC/ACPWM converters using voltage injection. IEEE Trans Ind Appl 44(5):1631–1637
36. Lee K, El-Sharkawi M (2008) Modern heuristic optimization techniques. Wiley, Hoboken, N.J.
37. Eltamaly AM, Al-Saud MS, Abo-Khalil AG (2020) Performance improvement of PV systems, maximum power point tracker based on a scanning PSO particle strategy. Sustainability 12(3):1185
38. Abo-Khalil AG, Alyami S, Alhejji A, Awan AB (2019) Real-time reliability monitoring of DC-link capacitors in back-to-back converters. Energies 12(12):1907

39. Eltamaly A, Al-Saud M, AboKhalil AG, Farah H (2019) Photovoltaic maximum power point tracking under dynamic partial shading changes by novel adaptive particle swarm optimization strategy. Trans Inst Meas Control
40. Abokhalil AG (2019) Grid connection control of DFIG for variable speed wind turbines under turbulent conditions. Int J Renew Energy Res (IJRER) 9(3):1260–1271
41. Abo-Khalil AG, Alghamdi AS, Eltamaly AM, Al-Saud MS, Praveen RP, Sayed K, Bindu GR, Tlili I (2019) Design of state feedback current controller for fast synchronization of DFIG in wind power generation systems. Energies 12, 2427
42. Eltamaly AM, Alolah AI, Abdel-Rahman MH (2011) Improved simulation strategy for DFIG in wind energy applications. Int Rev Model Simul 4(2)